

Multiple bottle beams based on metasurface optical field modulation and their capture of multiple atoms

Xichun Zhang(张希纯), Wensheng Fu(付文升), Jinguang Lv(吕金光), Chong Zhang(张崇),Xin Zhao(赵鑫), Weiyan Li(李卫岩), and He Zhang(张贺)

Citation: Chin. Phys. B, 2022, 31 (**8**): 088103. DOI: 10.1088/1674-1056/ac4e06
Journal homepage: http://cpb.iphy.ac.cn; http://iopscience.iop.org/cpb

What follows is a list of articles you may be interested in

High efficiency and broad bandwidth terahertz vortex beam generation based on ultra-thin transmission Pancharatnam-Berry metasurfaces

Wenyu Li(李文宇), Guozhong Zhao(赵国忠), Tianhua Meng(孟田华), Ran Sun(孙然), and Jiaoyan Guo(郭姣艳)
Chin. Phys. B, 2021, 30 (**5**): 058103. DOI: 10.1088/1674-1056/abd75c

Ultra-wideband reflective polarization converter based on anisotropic metasurface

Jia-Liang Wu(吴家梁), Bao-Qin Lin(林宝勤), Xin-Yu Da(达新宇)
Chin. Phys. B, 2016, 25 (**8**): 088101. DOI: 10.1088/1674-1056/25/8/088101

Polarization-insensitive unidirectional spoof surface plasmon polaritons coupling by gradient metasurface

Hong-yu Shi(施宏宇), An-xue Zhang(张安学), Jian-zhong Chen(陈建忠), Jia-fu Wang(王甲富), Song Xia(夏颂), Zhuo Xu(徐卓)
Chin. Phys. B, 2016, 25 (**7**): 078105. DOI: 10.1088/1674-1056/25/7/078105

Ultra-wideband circular-polarization converter with micro-split Jerusalem-cross metasurfaces

Xi Gao(高喜), Xing-Yang Yu(余行阳), Wei-Ping Cao(曹卫平), Yan-Nan Jiang(姜彦南), Xin-Hua Yu(于新华)
Chin. Phys. B, 2016, 25 (**12**): 128102. DOI: 10.1088/1674-1056/25/12/128102

High-efficiency wideband flat focusing reflector mediated by metasurfaces

Yu Ji-Bao, Ma Hua, Wang Jia-Fu, Li Yong-Feng, Feng Ming-De, Qu Shao-Bo
Chin. Phys. B, 2015, 24 (**9**): 098102. DOI: 10.1088/1674-1056/24/9/098102

Multiple bottle beams based on metasurface optical field modulation and their capture of multiple atoms

Xichun Zhang(张希纯)[1], Wensheng Fu(付文升)[1], Jinguang Lv(吕金光)[2], Chong Zhang(张崇)[3], Xin Zhao(赵鑫)[1], Weiyan Li(李卫岩)[1], and He Zhang(张贺)[1,†]

[1] *State Key Laboratory of High Power Semiconductor Lasers, Changchun University of Science and Technology, Changchun* 130022, *China*
[2] *State Key Laboratory of Applied Optics, Changchun Institute of Optics, Fine Mechanics and Physics, Chinese Academy of Sciences, Changchun* 130033, *China*
[3] *The First Military Representative Office of the Army in Changchun, Changchun* 130033, *China*

(Received 26 October 2021; revised manuscript received 30 December 2021; accepted manuscript online 24 January 2022)

Compared to conventional devices, metasurfaces offer the advantages of being lightweight, with planarization and tuning flexibility. This provides a new way to integrate and miniaturize optical systems. In this paper, a metasurface capable of generating multiple bottle beams was designed. Based on the Pancharatnam–Berry (P–B) phase principle, the metasurface lens can accurately control the wavefront by adjusting the aspect ratio of the titanium dioxide nanopillars and the rotation angle. When irradiated by left-handed circularly polarized light with a wavelength of 632.8 nm, the optical system can produce multiple micron bottle beams. Taking two bottle beams as examples, the longitudinal full widths at half-maximum of the optical tweezers can reach 0.85 μm and 1.12 μm, respectively, and the transverse full widths at half-maximum can reach 0.46 μm and 0.6 μm. Also, the number of generated bottle beams can be varied by controlling the size of the annular obstacle. By changing the x-component of the unit rotation angle, the metasurface can also change the shape of the bottle beam — the beam cross-section can be changed from circular to elliptical. This paper also analyzes the trapping of ytterbium atoms by the multi bottle beam acting as optical tweezers. It is found that the multi bottle beam can cool and trap multiple ytterbium atoms.

Keywords: metasurface, bottle beam, optical tweezers, Pancharatnam–Berry phase

PACS: 81.05.Xj, 41.85.–p, 87.64.M–, 03.65.Vf **DOI:** 10.1088/1674-1056/ac4e06

1. Introduction

A bottle beam is a special hollow beam with a closed dark field in three dimensions along the propagation direction. This dark field is a closed region surrounded by high-intensity light.[1,2] Bottle beams have a wide range of applications in optical tweezers,[3,4] laser catheters,[5] and optical micromanipulation.[6] In particular, when a bottle beam is applied to optical tweezers, it can stably capture and manipulate microscopic particles. Optical tweezers technology using a bottle beam as the light source has the advantages of non-contact and no strong light directly irradiating on the manipulated particles, so the particles can be manipulated without damage. Since 1987, various methods have been tried to generate bottle beams, such as the ring-slit-lens method,[7] the axial prism-lens system method,[7] the double-beam interferometry method,[9] the optical holography method,[10] and the phase plate method.[11]

With the Pancharatnam–Berry (P–B) phase metasurface proposed by Prof. Cappasso of Harvard University in 2012,[12] the study of metasurfaces has become a research hotspot in the international academic community today. The P–B phase metasurface usually consists of subwavelength-sized grating, and rectangular or elliptical anisotropic units arranged in a particular pattern. By rotating these units to a certain angle, the phase of the incident light can be changed locally, so that the amplitude, phase and polarization of the incident or reflected light can be manipulated arbitrarily,[13–17] thereby shaping the wavefront of the beam. Therefore, such optical devices can replace or improve conventional optical elements.[18–21] An important application in this regard is optical lenses based on metasurfaces. In 2019, Wu *et al.* designed a metasurface to generate 3D hollow spots and simulated the light field distribution of 3D hollow spots at different wavelengths.[22] In 2021, Li *et al.* integrated optical tweezers and optical spanners, using a metasurface to generate both optical tweezers and optical spanners. They enhance the application of metasurfaces as optical lenses.[23] For example, a metallic and dielectric-type-based metasurface has been used to focus light into the near or far field,[21–26] and even to achieve achromatic effects in the visible or infrared wavelength range.[27–29]

In this paper, we designed a metasurface with silicon dioxide (SiO_2) as the substrate and titanium dioxide (TiO_2) nanopillars as the unit. The incident light field passes through the metasurface to generate spherical waves and Bessel beam interference,[30] resulting in multiple high-intensity and micron-sized bottle beams. Compared to conventional optical systems, this system is simple and highly integrated. The lateral and longitudinal inner diameters of the generated bottle

†Corresponding author. E-mail: zhanghe@cust.edu.cn
© 2022 Chinese Physical Society and IOP Publishing Ltd

beam are significantly reduced. And the paper analyses the ability of the multiple bottle beams to act as arrayed optical tweezers, demonstrating their ability to capture multiple ytterbium atoms.

2. Metasurface design principles

2.1. Optical system design

As shown in Fig. 1, the design of the metasurface optical system is presented in this paper. The incident beam of the He–Ne laser is collimated using a collimator. The beam passes through a polarizer to produce linearly polarized light and then passes through a $\lambda/4$ waveplate to produce a left-rotating circularly polarized beam (the angle of the fast axis of the $\lambda/4$ waveplate needs to be 45° to the polarization direction of the polarizer to produce a left-rotating circularly polarized beam). Finally, the beam is incident on the metasurface to produce multiple bottle beams, and the spot is observed using a CCD camera.

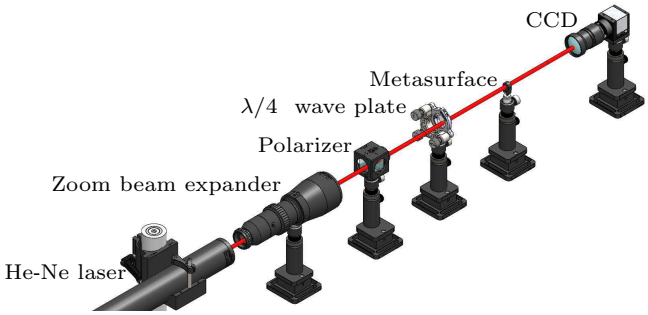


Fig. 1. A schematic diagram of the optical system.

2.2. Metasurface nanopillar design

When the circularly polarized light irradiates the P–B phase metasurface, the outgoing light will consist of two components: left-handed circularly polarized light and right-handed circularly polarized light. And the component of the outgoing light with the opposite spin direction of the incident light will carry the geometric phase delay ($\pm 2\theta$), where θ is the nanopillar unit rotation angle and ± 1 represents left-handed circularly polarized (LCP) and right-handed circularly polarized (RCP) light, respectively.

With regard to the substrate of the metasurface, high transmittance at the operating wavelength is required to reduce losses and improve the efficiency of the device. To build metasurface nanostructures, materials with both high transmittance and a high refractive index are required. For the above reasons, titanium dioxide (TiO_2) nanopillars arranged on a silicon dioxide (SiO_2) substrate are chosen in this paper. Both materials have high transmittance at 632.8 nm, where TiO_2 meets the two conditions of a sufficiently high refractive index and enough low loss rate in the working wavelength. The simulations were carried out using the commercial software package "finite-difference time domain (FDTD Solutions)" (Lumerical Inc.). When calculating the transmittance, polarization conversion and Pancharatnam–Berry phase of the cell, periodic boundary conditions are used along the x and y axes and the perfectly matched layer (PML) along the z-axis. The refractive indices of the SiO_2 substrate and TiO_2 cell are set to 1.46 and 2.58, respectively. To design the working wavelength of the metasurface as 632.8 nm, the metasurface nanopillar unit is shown in Fig. 2(a), and its length l, width w, and height h are selected as 377 nm, 87 nm, and 600 nm, respectively. Its polarization conversion efficiency, as well as transmittance, are higher than 85%. Here, the polarization conversion efficiency is defined as the ratio of the intensity of the transmitted light opposite the incident light rotation to the intensity of the incident circularly polarized light. And its P–B phase delay with the rotation of the nanopillar can cover 0–2π, so that it can effectively control the wavefront. The simulation results are shown in Fig. 2(b).

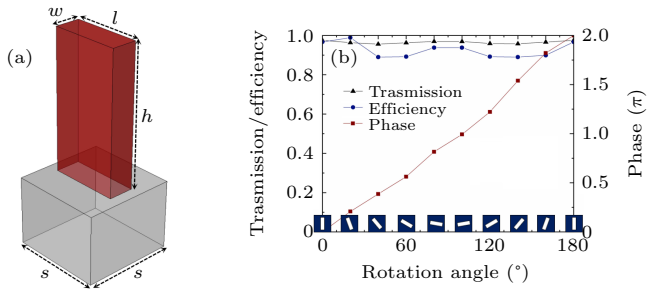


Fig. 2. A schematic diagram of the nanopillar unit and the relationship between its rotation angle and related parameters. (a) A schematic diagram of a single nanopillar unit. (b) The relationship between the rotation angle of the nanopillar unit and the transmittance (triangular line), polarization conversion efficiency (circular line), and P–B phase (square line).

2.3. Phase distribution of the metasurface

In this paper, the metasurface comprises three parts from inside to outside: an inner ring, an opaque ring obstacle, and an outer ring, as shown in Fig. 3, and their radii are $R_1 = 4$ μm, $R_2 = 6$ μm, and $R_3 = 2$ μm, respectively. For the inner ring part, the metasurface elements are arranged according to the hyperboloid phase distribution. Under the irradiation of left-handed circularly polarized (LCP) light, the generated waves interfere with the phase length in the focal plane, forming a focused light and acting as a convex lens. The arrangement is given by the following expression:[12]

$$\varphi_1(x,y) = \frac{2\pi}{\lambda}\left(\sqrt{(x^2+y^2)+f^2} - f\right), \quad (0 < R \le R_1), \quad (1)$$

where φ_1 represents the phase delay, λ is the incident wavelength, f is the given focal length, x and y are the transverse and longitudinal coordinates of the nanopillar centroid, respectively, and R is the metasurface radius. The phase delay can be achieved by rotating the nano cells based on the P–B phase

principle, and the expression for the rotation angle of the rectangular nanopillar on the metasurface is

$$\theta_1(x,y) = \frac{\pi}{\lambda}\left(\sqrt{(x^2+y^2)+f^2}-f\right), \quad (0<R\le R_1), \quad (2)$$

where θ_1 is the rectangular nanopillar rotation angle, and the relationship between the phase delay $\varphi_1(x,y)$ and the rectangular pillar cell rotation angle $\theta_1(x,y)$ is $\varphi_1(x,y) = 2\theta_1(x,y)$. For the outer ring part, which plays the role of an axicon, the metasurface units are arranged following a conical phase distribution to form a Bessel light. The cell arrangement is given by the following expression:[30]

$$\varphi_2(x,y) = \frac{2\pi}{\lambda}\sqrt{(x^2+y^2)}\sin\alpha, \quad ((R_1+R_2)<R\le R_4), \quad (3)$$

where α denotes the angle between the incident ray and the optical axis. Its unit rotation angle expression is

$$\theta_2(x,y) = \frac{\pi}{\lambda}\sqrt{(x^2+y^2)}\sin\alpha, \quad ((R_1+R_2)<R\le R_4). \quad (4)$$

In this paper, the metasurface radius $R_4 = 12$ μm, the focal distance $f = 10$ μm in the inner ring part, and the angle $\alpha = 0.75$ in the outer ring part (Fig. 3), composed of 1178 TiO_2 units. Its nano unit rotation angle is given by Eqs. (2) and (4).

Figures 4(a)–4(c) show two-dimensional schematic diagrams of the inner and outer ring parts and the ring obstacle metasurface, respectively. Schematic diagrams of the spherical wave and Bessel light distribution along the optical axis direction are shown in Figs. 4(d) and 4(e), respectively. The spherical wave generated in the inner ring part of the metasurface is coherently superimposed with the Bessel light generated in the outer ring part. Multiple high-intensity bottle beams are formed in the region of coherent superposition of the two beams. As seen in Fig. 4(f), four complete bottle beams are produced. Figures 4(g)–4(i) show the line distribution schematic of Figs. 4(d)–4(i), respectively.

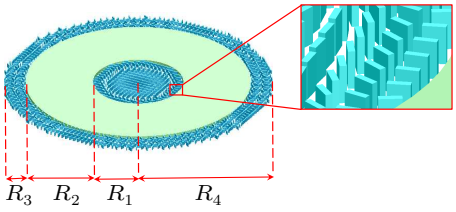


Fig. 3. A schematic diagram of the ring obstacle metasurface. The inset part is an enlarged view of the metasurface.

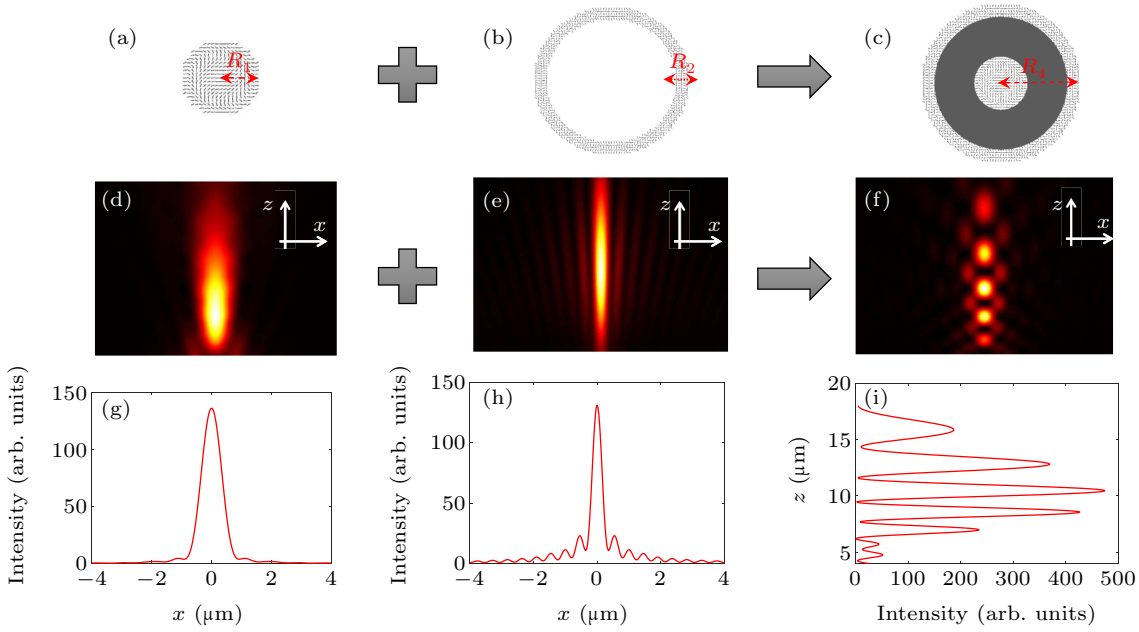


Fig. 4. The inner and outer rings of the metasurface, light field distribution and linear distribution. (a) A schematic diagram of the inner ring part of the metasurface. (b) A schematic diagram of the outer ring part of the metasurface. (c) A two-dimensional schematic diagram of the annular obstacle metasurface. (d) Optical field distribution of the spherical wave generated in the inner ring part. (e) Light field distribution of the Bessel light generated in the outer ring part. (f) Light field distribution of the bottle beam. (g) Line distribution of the spherical wave (d). (h) Line distribution of the Bessel light (e). (i) Line shape distribution of the multiple bottle beam (f).

3. Analysis and discussion

3.1. Bottle beam light field distribution

In this paper, a metasurface with a radius of 12 μm is designed and the incident light is LCP light. After simulation, four complete bottle beams are produced, labeled as Nos. 1, 2, 3, and 4 in this paper. The light field distribution of its beam propagation direction is shown in Fig. 5(a), and the cross-sectional light intensity of the multiple bottle beams at the propagation distances of 9.17 μm and 11.24 μm (at the focal plane of the bottle beams of Nos. 2 and 3) are shown in the small figure of Fig. 5(a). These two bottle beams were se-

lected, and the transverse full-widths at half-maximum of the two beams were measured to be 0.46 μm and 0.6 μm, and the longitudinal full-widths at half-maximum were 0.85 μm and 1.12 μm, respectively (as shown in Figs. 5(b)–5(d)). Here, the lateral and radial full-widths at half-maximum (FWHM) are defined as the distance between two points at half of the maximum intensity of the light field along the x and z directions of a single bottle beam.

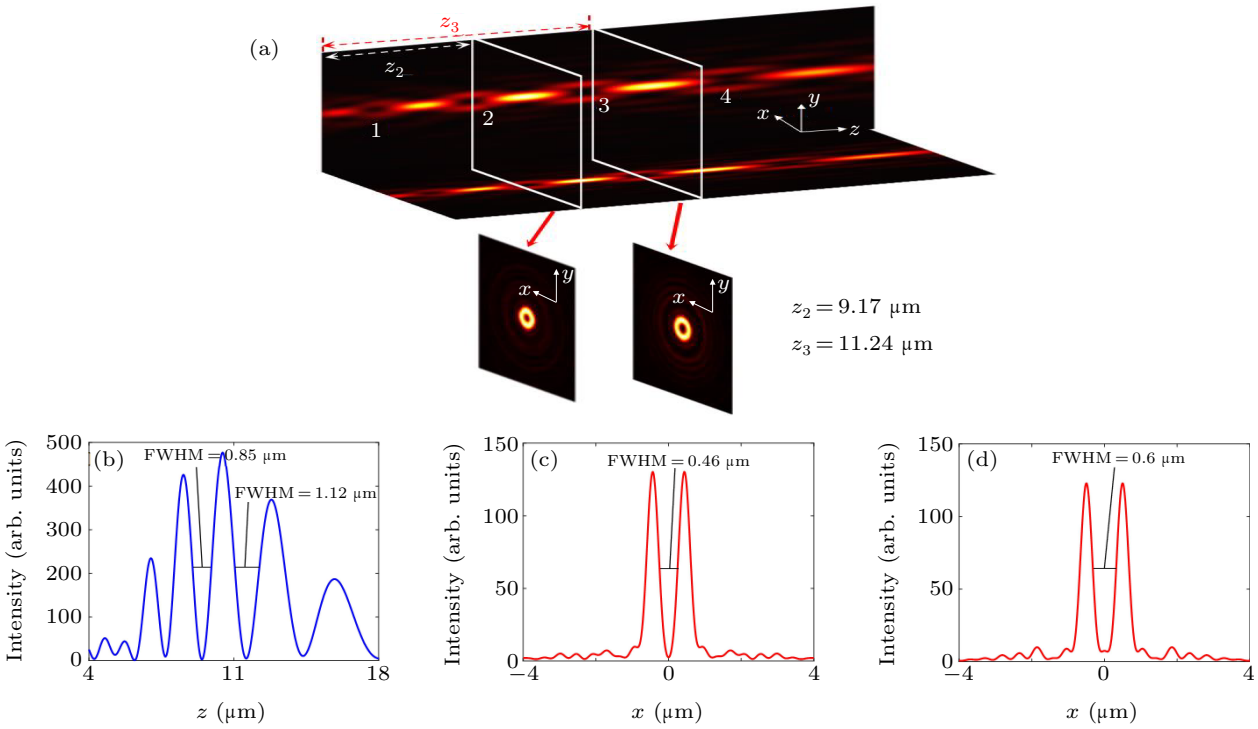


Fig. 5. A light field diagram and a linearity diagram of the multiple bottle beams. (a) Light field distribution in the beam propagation direction (z-direction) of the multiple bottle beams. The two insets show the transverse light field distributions at 9.17 μm and 11.24 μm, respectively. (b) Line distribution of the light intensity in the z-direction of the beam of the multiple bottle beams. (c), (d) Line distribution of the x-direction light intensity at 9.17 μm and 11.24 μm. The longitudinal full-widths at half-maximum (FWHM) of the bottle beams of 2 and 3 are 0.85 μm and 1.12 μm, respectively, and the transverse full-widths at half-maximum (FWHM) are 0.46 μm and 0.6 μm, respectively.

3.2. Effect of different aperture ring diaphragms on the number of bottle beams

The number of generated multiple bottle beams can be changed when the size of the annular obstacle on the metasurface. In this paper, the radius of the metasurface is 12 μm, and we control its outer ring size $R_3 = 2$ μm, and change the size of the ring obstacle so that the ring obstacle sizes are $R_2 = 5$ μm, 6 μm, and 7 μm, respectively (R_2 corresponds to Figs. 6(a)–6(c), respectively). Through simulation, from the figure, it is easy to find that the number of bottle beams is 2, 4, and 5 from left to right, respectively. When the focal length of the metasurface is constant, the size of the generated light field can be reduced by increasing the radius of the metasurface, allowing the light to be more focused. Therefore, when the inner ring of the focused light generated from Figs. 6(a)–6(c) gradually decreases, the size of the focused light gradually increases. The interference range between the focused light and Bessel light gradually increases, and the number of bottle beams generated increases in turn. Therefore, the number of bottle beams can be changed by controlling the size of annular obstacles on the metasurface. Then, the number of generated bottle beams can be designed according to the planned number of particles to be captured.

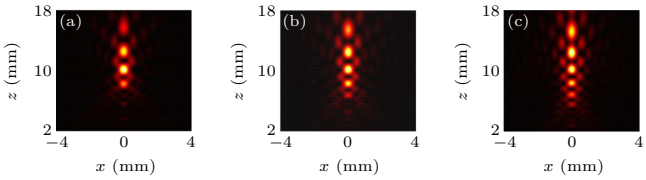


Fig. 6. The two-dimensional light field distribution along the beam propagation direction of the annular obstacle metasurface with different aperture sizes. From left to right, the annular obstacle dimensions are (a) $R_2 = 5$ μm, (b) $R_2 = 6$ μm, and (c) $R_2 = 7$ μm.

3.3. Effect of varying the x-component of the nanopillar unit on the shape of the bottle beam

When we change the x-directional component of the rotation angle of the nanopillar cell, the shape of the resulting bottle beam is changeable. Using a rounded corner rectangular opaque obstacle with a hollow circle in the center ($R_1 = 4$ μm, $R_4 = 12$ μm), as shown in Fig. 7, the metasurface is divided into three parts, numbered 1, 2, and 3 in Fig. 7. The second part of this is the hyperbolic phase distribution, whose focal plane light field distribution is shown in Fig. 7b, from which it can be seen that an elliptical light spot is formed, and the

rotation angle of the nanopillar unit on it is expressed by

$$\theta_3(x,y) = \frac{\pi}{\lambda}\left(\sqrt{\left((x/2)^2+y^2\right)+f^2}-f\right). \tag{5}$$

Parts 1 and 3 are tapered phase distributions with nanopillar units rotated at the angle shown in Eq. (4), producing a Bessel beam, as shown in small Fig. 7(a). Under the incidence of left-handed circularly polarized light, the elliptically focused light produced in part 2 interferes with the Bessel light produced in parts 1 and 3 to cancel. The resulting light field distribution is shown in Fig. 8.

Figures 8(a) and 8(b) show the light field distribution in the *xz* and *yz* directions, respectively. The cross-sectional light intensity of the multiple bottle beams at the propagation distances of 8.88 μm and 10.88 μm (at the white dashed lines in Figs. 8(a) and 8(b)) is shown in Figs. 8(c) and 8(d). These two bottle beams were selected, and the transverse full-widths at half-maximum of the No. 2 bottle beam were measured and found to be 0.46 μm and 0.98 μm (Fig. 8(c)), and the transverse full-widths at half-maximum of the No. 3 bottle beam were 0.54 μm and 1.3 μm (Fig. 8(d)). An elliptical bottle beam is obtained, which changes the shape of the beam and increases the versatility of its application.

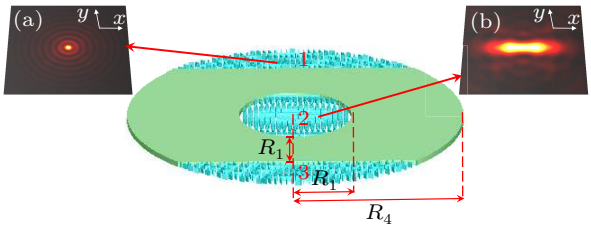


Fig. 7. (a) The hollow rounded rectangular obstacle metasurface, where the small figure (a) shows the focal plane of the Bessel beam generated in part 1 and the small figure (b) shows the focal plane of the focused light generated in part 2.

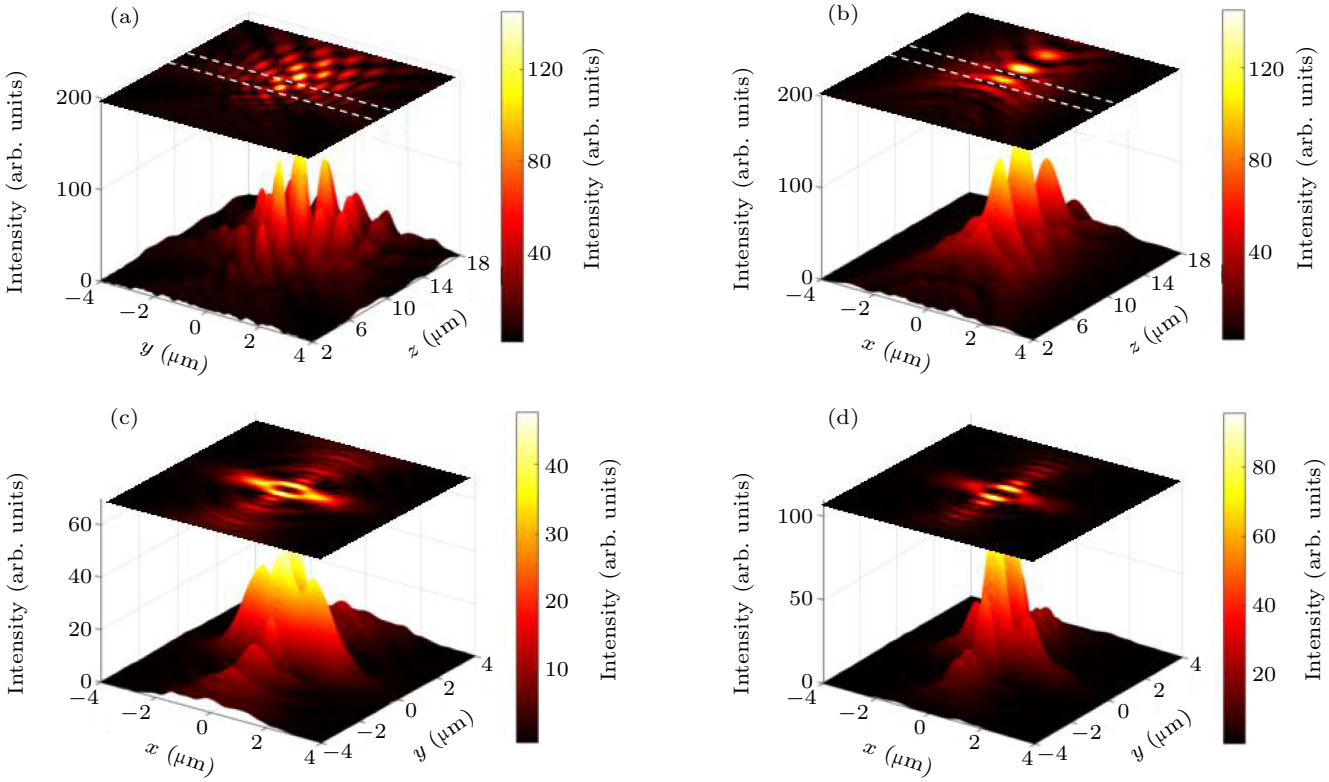


Fig. 8. (a), (b) Light field distribution of the multiple bottle beams in the *xz* and *yz* directions. (c), (d) Focal plane light intensity distribution of the multiple bottle beams at the propagation distances of 8.88 μm and 10.88 μm (at the white lines of beams 2 and 3), respectively.

4. Multiple bottle beams to capture multiple particles

4.1. Analysis of the radiation force on the particle

Since the bottle beam can be used as optical tweezers, this paper analyzes the radiation force and the feasibility of trapping multiple particles in the bottle light field of this array.

Usually, cooling and trapping atoms can be achieved by techniques such as cavity cooling,[31] Raman sideband cooling,[32] feedback cooling,[33] and intensity gradient cooling.[34] However, the size of the single-atom confinement potential trap produced by these schemes is relatively large, tens of thousands of times larger than the size of an atom, which makes the detection and subsequent application of single atoms more difficult. In contrast, the bottle beam generated in this paper has a small inner diameter size and a small captive region, so it can capture atoms more precisely. We chose the ytterbium atom (Yb) as the model of the imprisoned parti-

cle for the calculation, which is currently used in optical lattice clocks,[35] mainly for precise time measurement. This paper will analyze the ability of the bottle beam to trap ytterbium atoms, and provide an alternative method for atom cooling and trapping in ytterbium atomic optical lattice clocks.

Optical tweezers can capture two types of particles; one is a particle whose refractive index is greater than the refractive index of the surrounding medium, which is referred to as a class A particle. The other is a particle whose refractive index is less than the refractive index of the medium surrounding the particle, which is referred to as a class B particle. Generally speaking, the central bright spot formed by focusing the light beam can capture class A particles. And to stably capture class B particles, a bottle beam needs to be formed. In this paper, we consider capturing particles whose refractive indexes are smaller than the refractive index of the medium surrounding the particles, i.e., class B particles. The use of a bottle beam allows the particles to be controlled at a lower light intensity location, minimizing the effect of the beam energy on the particles.

In this paper, the Rayleigh scattering model is used to analyze the forces on the particles.[36] In this model, the particle can be viewed as a single dipole (a Rayleigh microsphere with a radius much smaller than the incident wavelength is considered as a dipole). The force acting on the particle is the force acting on the dipoles, and the force exerted by the optical field on this dipole can be divided into two parts, namely, the scattering force (F_{scat}) and the gradient force (F_{grad}).

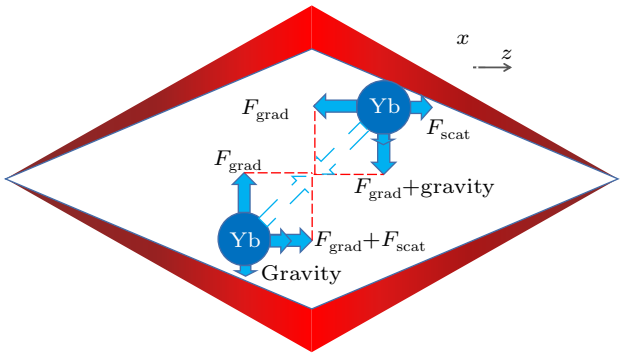


Fig. 9. A schematic diagram of the forces on ytterbium atoms in a bottle beam.

Figure 9 shows the transverse and longitudinal forces on two ytterbium atoms in different positions in the localized hollow beam. It can be seen from the figure that the combined forces (dashed arrows in Fig. 9) both point to the center of the hollow region, which leads to the capture of the atoms. The scattering force in the figure is caused by the absorption and re-radiation between the dipole of the beam in the direction of light transmission. The expressions are

$$F_{\text{scat}} = \left(\frac{n^2\varepsilon}{2}\right) CI, \tag{6}$$

where n is the refractive index of the medium (in this paper, we take $n = 1.332$ for water), $\varepsilon = 8.85 \times 10^{-12}$ is the dielectric constant in vacuum, and C is the cross-section of the atomic radiation pressure, which is expressed as

$$C = \frac{8}{3}\pi (ka)^4 a^2 \left(\frac{m^2-1}{m^2+2}\right)^2, \tag{7}$$

where $k = 2\pi/\lambda$ denotes the wave vector, the wavelength λ is 632.8 nm, and $a = 0.175$ nm is the ytterbium atomic radius. Here, $m = n_1/n$, where n_1 is the atomic refractive index.

$$F_{\text{grad}} = \frac{2\pi n a^3}{c}\left(\frac{m^2-1}{m^2+2}\right)\nabla I. \tag{8}$$

Here, c is the speed of light propagation in a vacuum.

Based on Eqs. (6)–(8), the gradient force and scattering force distributions of the multiple bottle optical field on ytterbium atoms are calculated, as shown in Fig. 10.

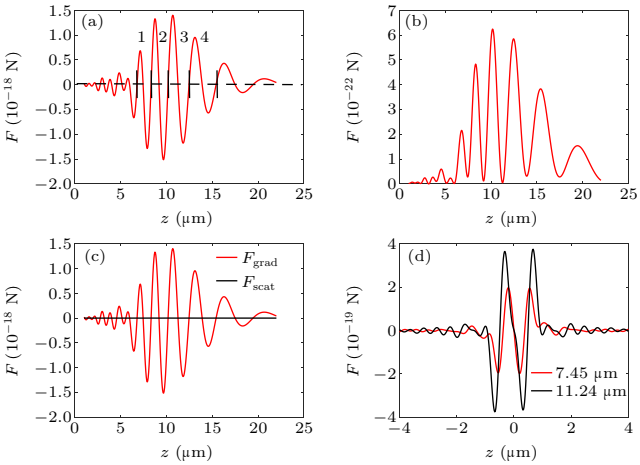


Fig. 10. The gradient force and scattering force distribution of multiple bottle beams. (a) Radial gradient force distribution. (b) Radial scattering force distribution. (c) A comparison of radial gradient force and radial scattering force. (d) Transverse gradient force distribution at 7.45 μm and 11.24 μm.

Figure 10(a) shows the distribution of the radial gradient force (z-direction): the gradient force is 0 at the black dashed line, and the black solid line marks the range where the bottle beams of 1, 2, 3, and 4 are located. The region where the radial gradient force is greater than 0 means that the direction of the gradient force is in the z-axis positive direction; in contrast, the region where the radial gradient force is less than 0 means that the direction of the gradient force is in the z-axis negative direction. Therefore, it can be seen from the figure that gradient force balance points exist in all four bottle light regions. Figure 10(b) shows the radial scattering force distribution. Figure 10(c) shows the radial gradient force compared with the radial scattering force, where the red line is the radial gradient force, and the black line is the radial scattering force. The scattering force is 5 orders of magnitude smaller than the gradient force, as can be seen from the figure. Therefore, the effect of the scattering force is minimal compared to the gradient force. Figure 10(d) shows the distribution of the transverse

gradient force at 7.45 μm and 11.24 μm (beams 2 and 4). Similarly, a transverse gradient force greater than 0 means that the direction of the gradient force is in the positive direction of the x-axis, and a transverse gradient force less than 0 means that the direction of the gradient force is in the negative direction of the x-axis. It can be seen from the figure that there is a transverse gradient force balance point at the center point ($x = 0$). Gradient force equilibrium points in both transverse and radial light fields imply that the atoms can be imprisoned. Here, the transverse and radial forces are defined as the forces exerted on the particle along the x and z directions, respectively.

4.2. Feasibility analysis of multiple bottle optical field imprisoned particles

To achieve stable capture of atoms, three stability criteria need to be satisfied.

1. The gradient force needs to be greater than the scattering force. The particle capture mainly relies on the gradient force generated by the optical field. We use the stability factor R to express the ratio of the gradient force and the scattering force, and its expression is

$$R = \frac{|F_{\text{grad}}|_{\max}}{|F_{\text{scat}}|_{\max}} > 1. \tag{9}$$

2. Another factor that affects the stability of the beam to enable it to capture particles is the Brownian motion of the particles, which affects the stability of the capture when the size of the particles being manipulated is small. Therefore, to capture the particles stably, the potential well generated by the gradient force should be deep enough to overcome the kinetic energy of the particles. In other words, the kinetic energy of the particle must be much smaller than the potential trapping well, which is expressed as

$$R_{\text{t}} = \text{e}^{(-U_{\max}/kT)} \ll 1. \tag{10}$$

Here, $U_{\max}$ denotes the maximum depth of the potential well, and its expression is $U_{\max} = |\text{Re}(\gamma)\varepsilon I_{\max}|$. γ denotes the polarization rate of the atom, and kT denotes the kinetic energy of the particle, where k is the Boltzmann constant and T is the temperature of the surrounding medium, which is taken as 300 K in this paper.

Here, the ytterbium atom is equated to a dipole, whose polarization rate can be described as

$$\gamma = 4\pi a^3 \varepsilon_1 (\varepsilon_2 - \varepsilon_1)/(\varepsilon_2 + 2\varepsilon_1), \tag{11}$$

where $\varepsilon_1 = 1.796$ is the dielectric constant of the environment surrounding the atom. Here, $\varepsilon_2 = -54 + 5.9\text{i}$ is the dielectric constant of the ytterbium atom.

3. The gradient force can balance the gravity of the particles. Therefore, the gradient force needs to be larger than the gravity of the particles.

In this paper, the bottle beams of Nos. 1 and 3 are selected to calculate their gradient forces and scattering forces. Also, the feasibility of trapping multiple ytterbium atoms is calculated. Since the scattering force is transmitted in the direction of light transmission (radial direction), there is no scattering force distribution in the lateral movement, so the stability criterion of (1) only needs to analyze the force in the radial direction. For bottle beam No. 1, it is calculated that: (1) the stability factor $R_1 = 2642.7$ yields a radial gradient force four orders of magnitude larger than the radial scattering force; (2) the beam radial $R_{\text{t1}} = 5.74\text{e}^{-22}$ and transverse $R_{\text{t1}} = 1.87\text{e}^{-5}$, both much smaller than 1, indicate that the potential trap generated by the gradient force is sufficient to overcome the kinetic energy generated by the Brownian motion of the atoms; (3) gravity $G = 2.82\text{e}^{-24}$ is six orders of magnitude smaller than the gradient force, and gravity can be neglected. Therefore, stable confinement can be achieved for the No. 1 bottle beam.

For the No. 3 bottle beam, it is calculated that: (1) the stability factor $R_2 = 2242.7$; (2) the beam radial $R_{\text{t2}} = 4.2147\text{e}^{-28}$ and the beam transverse $R_{\text{t2}} = 5.19\text{e}^{-8}$; (3) gravity $G = 2.82\text{e}^{-24}$. By combining the three stability criteria, the No. 3 bottle beam can also achieve stable confinement. Therefore, both Nos. 1 and 3 bottle light fields can achieve cooling and captivity of ytterbium atoms, and the capture of multiple particles is achieved.

5. Conclusion

In this paper, the P–B phase metasurface is used to generate several micron-scale bottle beams. Two bottle beams are selected and their transverse full-widths at half-maximum are measured to be 0.46 μm and 0.6 μm, with longitudinal full-widths at half-maximum of 0.85 μm and 1.12 μm. The metasurface lens can change the number of bottle beams generated by controlling the size of the annular obstacle. And the shape of the focal point can be changed by changing the rotation of the x-component of the unit, which generates an elliptical bottle beam.

Two of the bottle beams are selected, and their ability to imprison Yb atoms is analyzed. By combining the three stability criteria, it is concluded that both bottle beams can cool and imprison the ytterbium atoms.

In practical applications, the metasurface is lighter, thinner, and easier to integrate. Moreover, the size of the multiple bottle beams generated in this paper is significantly reduced, resulting in more accurate capture of tiny particles. The multiple bottle beams will have applications in super-resolution microscopy, super-resolution lithography, high-density data storage, optical micromanipulation of nanoparticles, and nano-optical manufacturing.

Acknowledgment

Project supported by the State Key Laboratory of Applied Optics (Grant No. SKLA02020001A17).

References

[1] Ashkin A, Dziedzic J M and Yamane T 1987 *Nature* **330** 769
[2] Qiu P Z, Yu B B, Jing M, Lv T G, Lian J Q and Zhang D W 2018 *Appl. Phys. Exp.* **11** 072003
[3] Xu X and Nieto-Vesperinas M 2019 *Phys. Rev. Lett.* **123** 233902
[4] Xu X, Nieto-Vesperinas M, Qiu C W, Liu X, Gao D, Zhang Y and Li B 2020 *Laser Photon. Rev.* **14** 1900265
[5] Snakard E P, Miller M, Berridge B, Gowda A, McNichols R J and Fossum T 2001 *J. Invest. Surg.* **14** 357
[6] Stefan A E and Andersen P E 2010 *J. Biomed. Opt.* **15** 041501
[7] Durnin J, Miceli J and Eberly J H 1987 *Phys. Rev. Lett.* **58** 1499
[8] Wu F T, Lu W H and Ma B T 2009 *Acta Opt. Sin.* **29** 2557
[9] Isenhower L, Williams W, Dally A and Saffman M 2009 *Opt. Lett.* **34** 1159
[10] McGloin D, Spalding G C, Melville H W and Dholakia K 2003 *Opt. Lett.* **11** 158
[11] Ozeri R, Khaykovich L and Davidson N 1999 *Phys. Rev. A* **59** R1750
[12] Khorasaninejad M, Chen W T, Devlin R C, Oh J, Zhu A Y and Capasso F 2016 *Science* **352** 1190
[13] Zheludev N I and Kivshar Y S 2012 *Nat. Mater.* **11** 917
[14] Meinzer N, Barnes W L and Hooper I R 2014 *Nat. Photon.* **8** 889
[15] Yu N and Capasso F 2014 *Nat. Mater.* **13** 139
[16] Arbabi A, Horie Y, Bagheri M and Faraon A 2015 *Nat. Nanotechnol.* **10** 937
[17] Kruk S, Hopkins B, Kravchenko I I, Miroshnichenko A, Neshev D N and Kivshar Y S 2016 *APL Photon.* **1** 030801
[18] Fattal D, Li J, Peng Z, Fiorentino M and Beausoleil R G 2010 *Nat. Photon.* **4** 466
[19] Pfeiffer C and Grbic A 2013 *Phys. Rev. Lett.* **110** 197401
[20] Lin D, Fan P, Hasman E and Brongersma M L 2014 *Science* **345** 298
[21] Decker M, Staude I, Falkner M, Dominguez J, Neshev D N, Brener I and Kivshar Y S 2015 *Adv. Opt. Mater.* **3** 813
[22] Yin L, Vlasko-Vlasov V. K, Pearson J, Hiller J M, Hua J, Welp U and Kimball C W 2005 *Nano Lett.* **5** 1399
[23] Wu Z, Zhang Q, Jiang X, Wen Z, Liang G, Zhang Z, Shang Z G and Chen G 2019 *J. Phys. D: Appl. Phys.* **52** 415103
[24] Li T, Xu X, Fu B, Wang S, Li B, Wang Z and Zhu S 2021 *Photon. Res.* **9** 1062
[25] Liu Z, Steele J M, Srituravanich W, Pikus Y, Sun C and Zhang X 2005 *Nano Lett.* **5** 1726
[26] Huang F, Zheludev N and Chen Y 2007 *Appl. Phys. Lett.* **90** 091119
[27] Lu F, Sedgwick F G, Karagodsky V, Chase C and Chang-Hasnain C J 2010 *Opt. Exp.* **18** 12606
[28] Arbabi A, Horie Y, Ball A J, Bagheri M and Faraon A 2015 *Nat. Commun.* **6**
[29] Wang S, Wu P, Su V, Lai Y C, Chu C H, Chen J W and Tsai D P 2017 *Nat. Commun.* **8** 1
[30] Cheng Z M, Wu F T, Fang X, Fan D D and Zhu J Q 2012 *Acta Phys. Sin.* **61** 212 (in Chinese)
[31] Aieta F, Genevet P, Kats M A, Yu N, Blanchard R, Gaburro Z and Capasso F 2012 *Nano Lett.* **12** 4932
[32] Boozer A D, Boca A, Miller R, Northup T E and Kimble H 2006 *Phys. Rev. Lett.* **97** 083602
[33] Koch M, Sames C, Kubanek A, Apel M, Balbach M, Ourjoumtsev A, Pinkse P W H and Rempe G 2010 *Phys. Rev. Lett.* **105** 173003
[34] Yin Y L, Xia Y, Ren R M, Du X L and Yin J P 2015 *J. Phys. B: At. Mol. Opt. Phys.* **48** 195001
[35] Guo Hui L and Xin Ye X 2011 *Chin. Phys. Lett.* **28** 063203
[36] Harada Y and Asakura T 1996 *Opt. Commun.* **124** 529